PHILOSOPHICAL TRANSACTIONS A

rsta.royalsocietypublishing.org

Research

Cite this article: Richardson K, Bendtsen J. 2017 Photosynthetic oxygen production in a warmer ocean: the Sargasso Sea as a case study. *Phil. Trans. R. Soc. A* **375**: 20160329. http://dx.doi.org/10.1098/rsta.2016.0329

Accepted: 12 June 2017

One contribution of 11 to a discussion meeting issue 'Ocean ventilation and deoxygenation in a warming world'.

Subject Areas:
oceanography, biogeochemistry

Keywords:
photosynthesis, oxygen production, deep chlorophyll maximum, Sargasso Sea, eddy mixing, climate change

Author for correspondence:
Katherine Richardson
e-mail: kari@science.ku.dk

Photosynthetic oxygen production in a warmer ocean: the Sargasso Sea as a case study

Katherine Richardson[1] and Jørgen Bendtsen[2]

[1]Center for Macroecology, Evolution, and Climate, Natural History Museum of Denmark, University of Copenhagen, Copenhagen, Denmark
[2]ClimateLab, Symbion Science Park, Copenhagen, Denmark

JB, 0000-0003-1393-3072

Photosynthetic O_2 production can be an important source of oxygen in sub-surface ocean waters especially in permanently stratified oligotrophic regions of the ocean where O_2 produced in deep chlorophyll maxima (DCM) is not likely to be outgassed. Today, permanently stratified regions extend across approximately 40% of the global ocean and their extent is expected to increase in a warmer ocean. Thus, predicting future ocean oxygen conditions requires a better understanding of the potential response of photosynthetic oxygen production to a warmer ocean. Based on our own and published observations of water column processes in oligotrophic regions, we develop a one-dimensional water column model describing photosynthetic oxygen production in the Sargasso Sea to quantify the importance of photosynthesis for the downward flux of O_2 and examine how it may be influenced in a warmer ocean. Photosynthesis is driven in the model by vertical mixing of nutrients (including eddy-induced mixing) and diazotrophy and is found to substantially increase the downward O_2 flux relative to physical–chemical processes alone. Warming (2°C) surface waters does not significantly change oxygen production at the DCM. Nor does a 15% increase in re-mineralization rate (assuming $Q_{10} = 2$; 2°C warming) have significant effect on net sub-surface oxygen accumulation. However, changes in the relative production of particulate (POM) and dissolved organic material (DOM) generate

THE ROYAL SOCIETY PUBLISHING

relatively large changes in net sub-surface oxygen production. As POM/DOM production is a function of plankton community composition, this implies plankton biodiversity and food web structure may be important factors influencing O_2 production in a warmer ocean.

This article is part of the themed issue 'Ocean ventilation and deoxygenation in a warming world'.

1. Background

A large proportion (approx. 40%) [1] of the global ocean is more or less permanently stratified, which means that seasonal mixing processes are not sufficient to redistribute nutrients over the entire water column. This condition results in the surface ocean layer being permanently low in inorganic nutrients and such regions are, therefore, referred to as being *oligotrophic*. These oligotrophic regions occur at low latitudes and include the large sub-tropical gyres encountered in both the Atlantic and Pacific Oceans. Because surface waters in oligotrophic regions are characterized by low phytoplankton standing stock and low estimated rates of photosynthesis (low primary production (PP)), it is generally assumed that these low latitude regions represent the 'deserts' of the ocean. Several lines of evidence [2,3] suggest, however, that these regions may be more productive than commonly assumed and that it is photosynthesis at the base of the euphotic zone, well below the immediate surface layer, that drives primary production here [4,5]. As O_2 is a by-product of photosynthesis, such sub-surface production can be a potentially important mechanism for introducing O_2 to the water column in oligotrophic regions.

Indeed, one of the early studies [2] suggesting substantial (approx. $50\,g\,C\,m^{-2}\,yr^{-1}$) new production[1] to be occurring in the oligotrophic Sargasso Sea was based on the observation of a sub-surface region of elevated O_2 concentrations that they argued must be of photosynthetic origin. Accumulation of O_2 in the lower part of the euphotic zone and formation of a shallow oxygen maximum (SOM) are recognized features in the North Atlantic [2] and Pacific subtropical gyres [8]. This is also evident from climatological fields of apparent oxygen utilization (AOU) where negative values, i.e. production of oxygen (the effect from subsurface heating cannot account for the large negative signal), cover a large area of the central Sargasso Sea (figure 1). More recent studies [3,10] applying different methods to estimate export production have also suggested that substantial new photosynthetic production must be occurring in the water column in at least some permanently stratified oligotrophic regions. A conundrum here, however, is that direct measurements of photosynthetic/primary production rates based on ^{14}C uptake/nitrogen uptake in oligotrophic regions have generally failed to identify rates that could lead to the order of magnitude of O_2 accumulation observed and export estimates reported.

There are several potential explanations for the disagreement between direct measurements of photosynthetic rate and indirect estimates of seasonal new or export production rates in permanently stratified oligotrophic regions. Firstly, direct measurement of photosynthesis is made on small samples taken at discrete depths. Usually the depth/depths for determining photosynthesis rates are selected from surface waters and taken at fixed depths or levels of light penetration. Such sampling strategies do not necessarily include sampling at the depth of the deep chlorophyll maximum (DCM) which is consistently found in the deepest part of the euphotic zone, i.e. at depths below 100 m, in the Sargasso and other oligotrophic ocean areas.

Despite the fact that these DCM are found at the base of the euphotic zone and thus experience low ambient light intensities, there have been reports that photosynthesis at the DCM can contribute substantially to water column production in the Sargasso Sea [5,11]. ^{15}N and isotope analyses in surface waters in the Sargasso Sea suggest that nitrogen fixation (diazotrophy) is

[1]*New production* [6,7] is defined as photosynthesis based on an allochthanous nitrogen source. Only new production can lead to a net increase in organic material in the system and an accumulation of O_2. The *f*-ratio [7] refers to the percentage of new production occurring, i.e. new/total PP. Most new production will ultimately be exported from the system in which it is generated, i.e. *Export* production and *Export ratio* (*e*-ratio) represents export/total PP. At steady state, then, *e*-ratio becomes *f*-ratio.

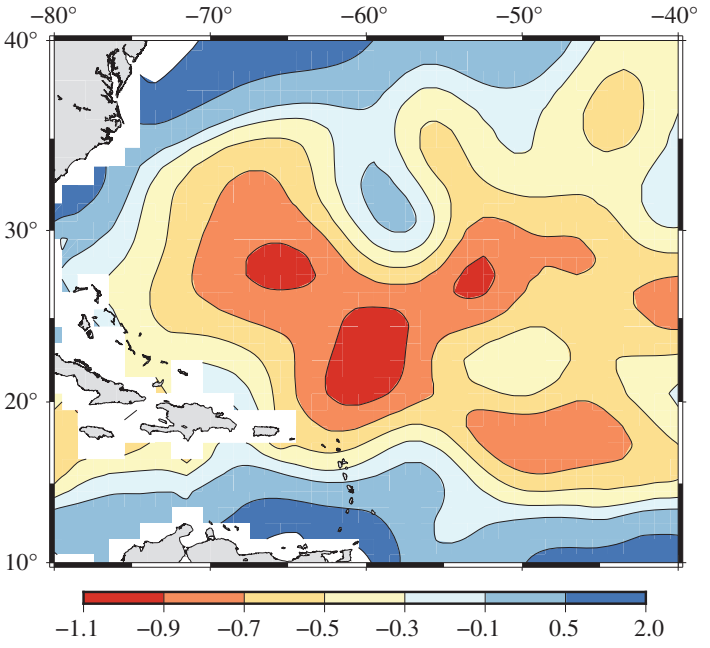

Figure 1. AOU in the Sargasso Sea. AOU (mmol O_2 m^{-3}) in September averaged in the depth interval between 80 and 30 m (WOA05 [9]). (Online version in colour.)

an important source of the nitrogen supporting photosynthesis in the upper part of the water column here [4,12,13]. However, Fawcett *et al*. [5] found the majority of new production taking place in the water column in the Sargasso Sea to be taking place near the nutricline, i.e. in association with the DCM, and that it was not based on diazotrophy but, rather, on the inorganic nutrients found here. These findings suggest that many of the reported studies examining water column photosynthesis in oligotrophic regions can have failed to sample what may be the most important vertical feature of photosynthesis in the oligotrophic water column.

Another possible explanation for the disagreement between discrete measurements of photosynthetic rates and estimates of export production in oligotrophic regions is that new production at the base of the euphotic zone may be occurring episodically over relatively small areas at any given time. Evidence for this postulate comes from studies of eddies in the sub-tropical gyres [14–17] indicating that vertical mixing associated with the passage of such eddies can potentially introduce a significant nutrient input from deep ocean waters to the lower regions of the euphotic zone. Richardson *et al*. [4] estimated vertical mixing between the nutricline and DCM along three transects in the Sargasso Sea and found a localized region with elevated vertical mixing in the depth ranges that potentially could transport nutrients from below the nutricline to the depth of the DCM. They estimated that nutrient delivery to the DCM here was an order of magnitude greater than outside of this localized mixing patch. Those authors also reported changes in plankton community responses consistent with relaxed nutrient limitation within this patch. Thus, in addition to much of the photosynthesis resulting in new production in the Sargasso Sea apparently occurring at the base of the euphotic zone, it may also be occurring in episodic 'bursts', making it even more difficult to directly detect.

Already today oligotrophic regions comprise a large proportion of the global ocean but their area is predicted to increase in response to global warming [1]. Thus, understanding primary production processes, i.e. the magnitude of new and export production and the role that photosynthesis may have in oxygenating the water column, as well as how these processes may be

influenced in a warmer ocean becomes a priority when trying to predict future ocean conditions. The IPCC AR5 WGI [18] concluded (medium confidence) that ocean primary production may decrease in stratified areas at low and mid-latitudes in response to climate change. However, processes potentially leading to new production at the base of the euphotic zone as described above would not be resolved in the current coupled climate–ocean biogeochemical Earth system models employed by the IPCC. There is, therefore, a need to revisit primary production in oligotrophic regions and how it may respond to a warmer ocean.

To do so, we first carried out field studies in the Sargasso Sea examining the vertical distribution of photosynthesis. The Sargasso Sea is located in the North Atlantic sub-tropical gyres. Subtropical gyres are present in all ocean basins and driven by the large-scale wind field between the westerlies at mid-latitudes and trade winds in the tropics. Thus, the general hydrography of these gyres is similar in the Atlantic, Pacific, and Indian Oceans [19]. Therefore, we believe our results for the Sargasso Sea to potentially also be relevant to the understanding of factors controlling photosynthesis and primary production in other regions characterized by sub-tropical gyres.

On the basis of hypotheses created from these newly collected data together with those previously reported in the literature, we develop a one-dimensional water column model describing photosynthetic oxygen production in the Sargasso Sea. The model suggests that photosynthetic oxygen production makes a quantitatively important contribution to oxygenation of the water column here. Furthermore, and in contrast to the conclusions of the IPCC, the model suggests that photosynthesis and its associated contribution to oxygenation of the water column are unlikely to decrease in a warmer ocean unless there is a change in the relative ratio in the photosynthetic production of particulate/dissolved organic material.

2. Material and methods

(a) Field programme

Conductivity, temperature and depth (CTD; Seabird SBE911 plus system with a SCUFA fluorometer) and underway CTD (UCTD) were carried out in the central Sargasso Sea in the period 16 March–5 April 2014 along four transects between 24.7 and 31.5° N along 68.50 (T1), 65.50 (T2), 62.50 (T3) and 62.75° W (T4) respectively, where standard CTD casts down to 400 m were made every approximately 50 km, and UCTD measurements were made between the CTD stations, also down to 400 m, with a horizontal spacing of approximately 7–11 km.

Water samples were taken at CTD stations from seven depths (10, 30, 60, 100, DCM, 200 and 400 m) and analysed for nutrients, chlorophyll *a* and variable fluorescence. The rosette was held at each sampling depth for 2 min (5 min at 100 m) before closing the Niskin bottles. Measurements from transects T1 and T4 are compared below.

(b) Nutrients, chlorophyll *a* and variable fluorescence

Water samples from all depths were tapped from 10 l Niskin bottles and immediately frozen. The seawater was subsequently filtered (Millipore Millex-GP Hydrophilic PESO 0.22 mm) and analysed for dissolved inorganic nitrogen (DIN) compounds, i.e. nitrate, nitrite and ammonium, via wet chemistry methods in accordance with [20], using a SanPlus System Scalar auto analyser at Aarhus University, Denmark. Water samples were also taken for salinity calibration (Portasal). Chlorophyll *a* measurements were made fluorometrically [21] following ethanol (96%) extraction of chlorophyll retained on a glass fibre filter (Whatman). These were used to calibrate CTD fluorescence ($n = 133$, $r^2 = 0.82$).

Variable fluorescence (F_v/F_m) was measured using a FASTTRACKA fluorometer (Chelsea Instruments Group Ltd). A single turnover protocol with 30 sequences per acquisition, each including 100 saturation flashlets and 20 relaxation flashlets, was used. The sequence interval was set to 1000 ms. F_v/F_m was calculated from a saturation phase fit and a relaxation phase

fit following [22]. Only measurements with a qualifying saturation phase and relaxation phase were included in the dataset. We have earlier shown [23] using data from this cruise that F_v/F_m determinations on samples taken from depths where the incident photosynthetic available radiation (PAR) is greater than approximately 200 µmol photons $m^{-2}\,s^{-1}$ contain a light history signal, presumably as a result of photoinhibition. Therefore, although all F_v/F_m values are presented, only those for samples taken from water depths where the incident light did not exceed 200 µE $m^{-2}\,s^{-1}$ during the 4 h prior to sampling are considered here when we compare the photosynthetic potential between phytoplankton at different depths.

(c) One-dimensional water column model

The seasonal oxygen dynamics in the central Sargasso Sea were studied with a one-dimensional water column model. The model is based on the COHERENS model system [24] and extended with a one-dimensional vertical advection operator to include the influence of passing eddies and a biogeochemical component.

Previous biogeochemical studies from subtropical oligotrophic gyres have shown that weak diapycnal mixing is, in general, insufficient to supply the euphotic zone with nutrients to explain primary and export production. Mesoscale eddies [14–16] and fixing of atmospheric nitrogen by diazotrophs [12,13] have on the other hand been suggested as potentially important processes for supplying the surface layer with nutrients. Observations of low ^{15}N-isotopic signatures in the particulate organic matter in the surface layer also suggest that N_2 fixation may be an important driver of planktonic food webs in the upper water column in the Sargasso Sea [4]. We explicitly include, therefore, both eddy mixing and diazotrophy in the model described below.

The water column model solves the vertically (z) time-dependent (t) one-dimensional transport equation for the various state variables (φ):

$$\frac{\partial \varphi}{\partial t} + w_{\mathrm{eddy}} \frac{\partial \varphi}{\partial z} = \frac{\partial}{\partial z} k_v \frac{\partial \varphi}{\partial z} + S(\varphi). \tag{2.1}$$

The vertical turbulent diffusion coefficient (k_v) is determined by a k–ε scheme ($k_v(k{-}\varepsilon)$) and a background diffusion (k_v(bg)) characterized by a constant of $1 \times 10^{-5}\,m^2\,s^{-1}$, in accordance with the general low background diapychnal mixing in the ocean interior [25]. The influence from mixing associated with passing mesoscale eddies (k_v(eddy)) is added to the mixing scheme so the turbulent diffusion coefficient is the sum of: $k_v = k_v(k-\varepsilon) + k_v(\mathrm{bg}) + k_v(\mathrm{eddy})$. In addition, the influence from mesoscale eddies is considered explicitly by extending the one-dimensional set-up of the COHERENS model to solve the vertical advection–diffusion equation with a specified vertical velocity due to eddies (w_{eddy}). The influence from passing eddies was considered by specifying a periodic eddy passage from cyclonic (anticyclonic) eddies, corresponding to upwelling (downwelling) of isopycnals with a period between passages of 80 days, a passage interval of 20 days, a sinusoidal vertical displacement with a maximum at mid-depth (200 m) of 64 m and an eddy-associated mixing (k_v(eddy)) related to the isopycnal heave rate (cf. appendix A).

The parameters characterizing vertical velocities and isopycnal displacements were based on observed spatial fluctuations associated with mesoscale structures and eddy mixing was assumed to scale linearly with vertical velocity and to have a maximum value of $5 \times 10^{-4}\,m^2\,s^{-1}$ at mid-depth. Such high vertical velocities and mixing rates have been associated with observed mesoscale frontal dynamics [4,16] and model sensitivity to this parametrization is analysed below. The model is driven by meteorological forcing from the central Sargasso Sea in 2014 and simulates temperature and salinity, where temporal salinity variations in the upper 150 m are considered in a simple data-assimilation scheme. In this manner, the influence of salinity on stratification is taken into account.

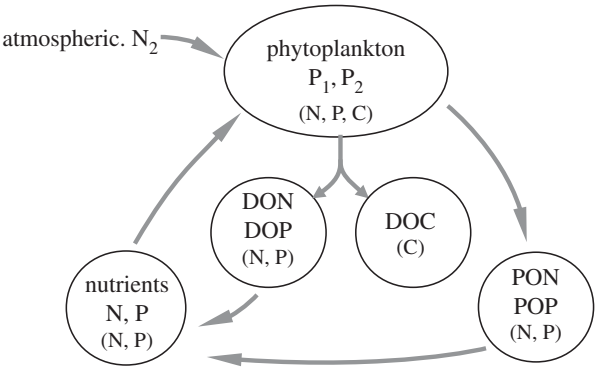

Figure 2. Biogeochemical model. Nitrogen (N), phosphorus (P) and carbon (C) cycling considering uptake of nutrients (N, P) and atmospheric N_2 by two phytoplankton groups (P_1 and a group of diazotrophs, P_2), production of particulate organic nitrogen and phosphorus (PON, POP) and dissolved pools of DON, DOC and PON. All organic pools are re-mineralized to inorganic nutrients.

(d) Biogeochemical model

A simple biogeochemical model simulating oxygen production and consumption from primary production and re-mineralization, respectively (figure 2) was developed. The model was configured to simulate primary production and oxygen cycling for the area with a minimum of complexity. Primary production is regulated by the chlorophyll *a* concentration of phytoplankton, PAR, photosynthetic parameters characterizing the metabolic efficiency of the phytoplankton cells (i.e. maximum rate (normalized to chlorophyll) of light saturated photosynthesis, P^{B}_{max}, and the slope of the photosynthesis (normalized to chlorophyll) versus light curve, α^{B}) and the surrounding nutrient concentrations. The individual model components are described in detail in appendices A and B.

3. Results and discussion

(a) Field studies

A DCM was observed on all transects (generally located between the 25.5 and 26.0 kg m^{-3} isopycnals) whereas low chlorophyll values were recorded towards the surface (figure 3*a*,*c*). The distribution of F_v/F_m exhibited a clear optimum in the DCM, implying that phytoplankton cells here had a higher capacity for electron transport in photosystem II than cells located higher in the water column. The average near-surface DIN values at 10 m depth along T1 and T4 of 0.52 ± 0.33 and 0.24 ± 0.21 µmol kg^{-1}, respectively, were slightly higher than deeper in the surface layer (figure 3*b*,*d*). This finding is consistent with a contribution from dinitrogen fixation by diazotrophs in near-surface waters. However, DIN was relatively low from the surface and down to 100 m. Average values at the depth of the DCM, located on both transects around 119 m, were approximately 0.6 and 0.4 µmol kg^{-1} on transects T1 and T4, respectively. The nutricline depth (DNO_3, defined here as the depth where DIN = 1 µmol kg^{-1}) was located at 140 m on both transects.

Despite the low ambient DIN concentrations recorded in and below the DCM, the higher F_v/F_m recorded in the DCM compared with depths above the DCM indicates that phytoplankton in the DCM are likely more nutrient replete than those found higher in the water column (figure 3*a*,*c*). This, in turn, suggests that phytoplankton in the DCM are gaining access to DIN from deeper in the water column. The isopycnal profiles for the upper 200 m on T1 and T4 suggest the possibility for vertical nutrient transport at depths relevant for nutrient delivery to the DCM on T1, e.g. associated with the isopycnal rise of more than 50 m at 150 depth seen at 27° N where a frontal zone between two mesoscale eddies was crossed (figure 3*a*).

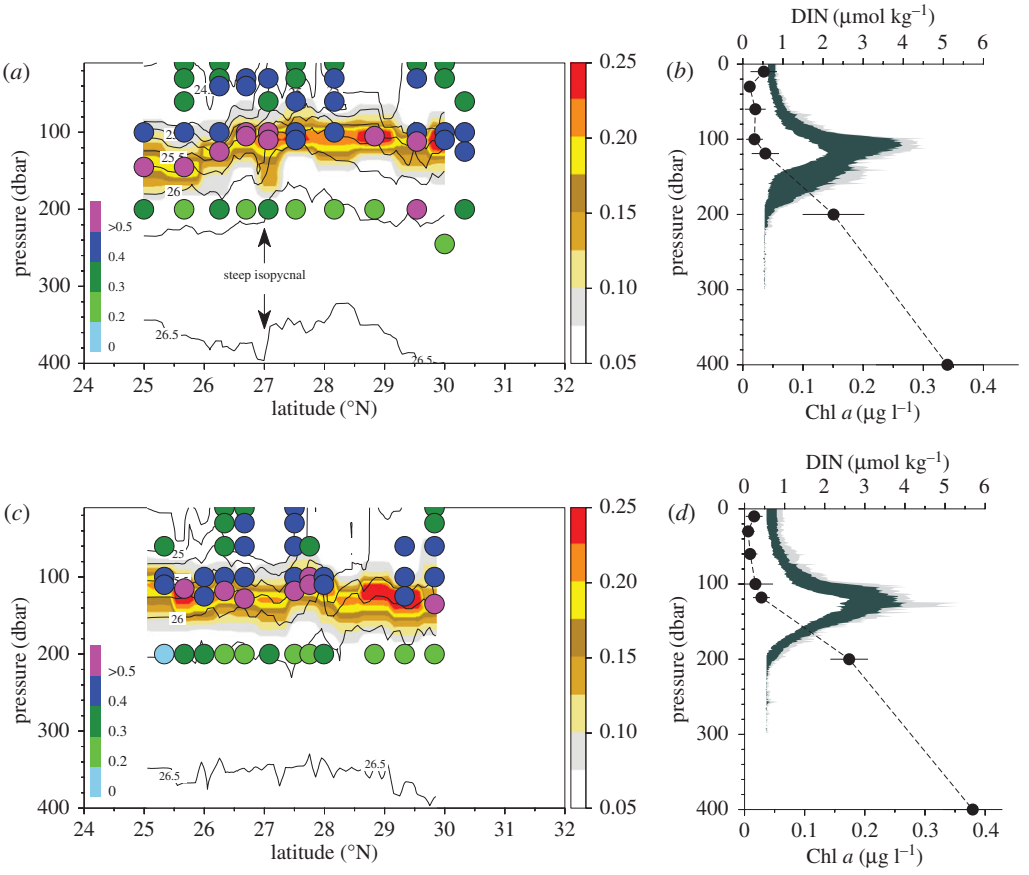

Figure 3. Observations from the central Sargasso Sea. Fluorescence (colours; µg l^{-1}) and σ_θ (contours; kg m^{-3}) along two transects (T) (*a*) T1 and (*c*) T4. Variable fluorescence (F_v/F_m) measurements are shown with bullets (left colour scale). Mean values (bullets, s.d.) of DIN along (*b*) T1 and (*d*) T4 and average fluorescence (grey, shading between ±s.d.) and maximum values (light grey). (Online version in colour.)

Marked horizontal heterogeneity was also noted in salinity in the 100–150 m depth range (not shown) on T1 at approximately 27° N, indicating significant lateral intrusions and sub-mesoscale mixing. Deep sub-mesoscale variability was identifiable due to the small horizontal distance between U/CTD stations. This same section of T1 coincided with a steep rise of isopycnals in the whole upper 400 m of the water column (see also 'steep isopycnal' labelled in figure 3*a*). Similar surface frontal signatures (i.e. changes in sea-surface temperature (SST) and sea-surface salinity) on deep isopycnals were not seen on transect T4 (figure 3*c*). Thus, the results of the field studies carried out here are consistent with findings suggesting a contribution by diazotrophy to DIN in the immediate surface layer of the water column and the potential for vertical transport of nutrients from below the nutricline to the DCM.

The most novel feature in the results from these field studies is the finding that highest values for F_v/F_m (a proxy for electron transport in photosystem II) in the water column are found in association with the DCM. F_v/F_m is an indicator of the average physiological state of the photosynthetic system in the phytoplankton community. The higher the F_v/F_m, the better the physiological state but F_v/F_m can vary as a function of the species present [26]. Therefore, this ratio cannot be used as an absolute indicator of physiological state. Nevertheless, when values are greater than approximately 0.4, good photosynthetic physiological condition can generally be assumed. F_v/F_m can be reduced as a function of both photo-damage to the photosynthetic system (photoinhibition) and nutrient depletion [27,28]. We have earlier shown [23] that phytoplankton

in this area at the time of this study were not experiencing photoinhibition at light intensities below approximately 200 µE m^{-2} s^{-1}. This means that low F_v/F_m recorded in samples taken from below approximately 50 m even at midday is most likely an indication of nutrient stress in the phytoplankton community.

That F_v/F_m values peak first at depths of around 100 m (figure 3) suggests that phytoplankton above these depths are nutrient stressed relative to the phytoplankton at the DCM and that phytoplankton in the DCM must have access to a nutrient source which is not available to the phytoplankton found in more shallow waters. In an earlier study [4], we found a patchy distribution of F_v/F_m in the DCM, where elevated values were recorded in association with localized vertical mixing assumed to be delivering more nutrients to the DCM here than in surrounding waters. In this study, however, the F_v/F_m values were high at depths of approximately 100 m over the entire study area. This suggests that all DCM phytoplankton in the study area must recently have experienced nutrient enrichment. Our finding that the DCM phytoplankton appear to be in a better physiological condition and have greater access to nutrients than phytoplankton at other depths in the water column lends strong support to studies [4,5] suggesting that photosynthesis at the base of the euphotic zone may be the major driver of new production in permanently stratified oligotrophic regions and calls for the development of a better understanding of PP in such regions.

(b) Model simulations of photosynthetic O_2 production in the Sargasso Sea

We explore relationships between the factors driving photosynthesis in the water column in the Sargasso Sea with the help of a one-dimensional water column model where the nitrogen necessary to drive photosynthesis is derived from either diazotrophy or processes leading to the transfer of nutrients from below the nutricline to the DCM. As model solutions when the model is run in its 'reference' state are in good agreement with known seasonal vertical distributions of temperature, nutrients, chlorophyll and oxygen in this area, we then use it to explore how water column changes induced by a warmer ocean might impact photosynthesis and oxygen production here.

(c) Reference case

(i) Seasonal thermocline

The model simulation of temperature in the reference case shows the deepening of the winter mixed layer until the start of March and the subsequent formation of a seasonal thermocline in the upper approximately 50 m. This is also seen from the shallow isoline of the turbulent diffusion coefficient between May and August (figure 4). The mixed layer depth generated by the model is in general accordance with climatology [29] during the stratified period and in the autumn. The climatological mixed layer depth is, however, a little deeper in January (approx. 70 m) than the 50 m simulated by the model. This can possibly be explained by a relatively warm surface forcing in 2014 compared with the climatological mean for the area. The model solution of data-assimilated salinity is tightly coupled to the climatological salinity field and shows the presence of high-saline subtropical underwater between 50 and 150 m depth from May and during the most strongly stratified period. Thus, lateral advection also plays a significant role for transporting substances in the upper 200 m in the area. Only vertical transports are considered in the model, i.e. advection of nutrients from surrounding areas is not included. The simulated primary and oxygen production may, therefore, represent underestimates compared with actual conditions.

The model simulates three eddy passages during the year and although the immediate influence from eddies leads to an isopycnal heave of about 40 m at the 100 m depth level, these have only a relatively small influence on the long-term displacements of the isopycnals, i.e. no significant depth changes of the isotherms are seen after the last two passages.

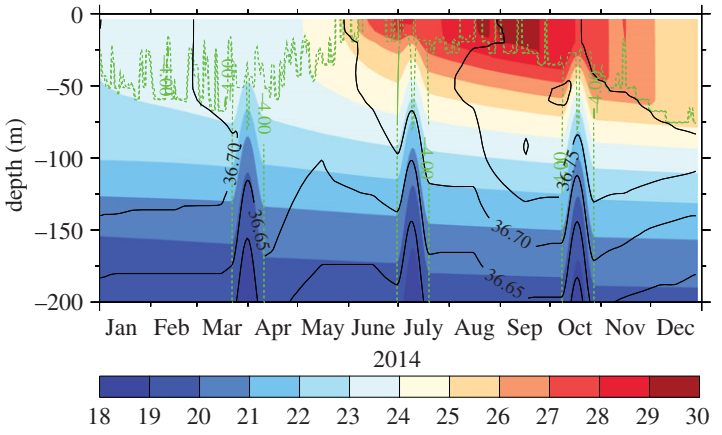

Figure 4. Reference simulation of temperature, salinity and mixing. Solution of temperature (colours, °C), assimilated background field of salinity (contours, black) and the vertical diffusion coefficient (k_v) (dashed contours of $\log_{10}(k_v)$). (Online version in colour.)

(ii) Primary production and the deep chlorophyll maxima

The simulated nitrate concentrations are relatively low in the upper 100 m during most of the year, whereas phosphorus concentrations first become depleted at the end of May (figure 5*a*). The model solution during early winter is sensitive to the initial conditions, i.e. the climatological fields, until the internal model dynamics redistribute the nutrients. However, it is interesting to note that phosphorus is in surplus compared with nitrate during most of the spring. The influence from the three cyclonic eddies causes a significant change in the nutrient distribution due to the relatively large vertical gradients above 100 m (i.e. isolines are shifted upwards after the eddy passages due to the relatively large vertical concentration gradients).

The relatively high initial oxygen concentration in January is homogenized in the upper 100 m during February and March. Photosynthesis leads to the formation of a SOM between 50 and 100 m depth from early spring (figure 5*b*). The DCM is significantly influenced by passing eddies and is seen to be displaced upwards following eddy passages and strengthened due to increased production generated by the eddy-induced nutrient input to the euphotic layer. Primary production increases during spring to approximately 80 mg C m^{-2} d^{-1} in April but decreases later in the year as stratification increases except in periods experiencing passage of eddies, when PP can increase to more than 100 mg C m^{-2} d^{-1} (figure 6*a*). Correspondingly, integrated water column chlorophyll *a* content increases to approximately 20 mg Chl *a* m^{-2} during spring. Eddy passages also cause a transient increase in water column chlorophyll *a* content. The simulated levels of PP and chlorophyll *a* are in general accordance with our observations from the area in 2007 [4,11] and 2014. Interestingly, the water column chlorophyll *a* content following eddy passages reaches its highest values later than the maximum in PP. This is due to growth of diazotrophs on the 'backside' of the eddies, where phosphorus has been introduced to the euphotic zone.

Photosynthetic production of oxygen remains relatively constant from spring to autumn. In total, 1.9 mol of O_2 is produced during the year (or approx. 0.22 mol N m^{-2} yr^{-1} in nitrogen-equivalents). Previous estimates from other localities in the Sargasso Sea and in the North Pacific subtropical gyre find a larger net oxygen production. Jenkins & Goldman [2] estimate about 0.6 mol N m^{-2} yr^{-1} in the period from April to August at a location further north (32° N) and Stanley *et al*. [3] obtain a similar estimate for the annual production at the Bermuda Atlantic Time-series Study (31.6° N). Thus, the model solution is significantly lower than these data-based estimates. This discrepancy could be explained by a significant advective transport of nutrients or labile organic material or a more efficient eddy transport of nutrients than applied in the reference

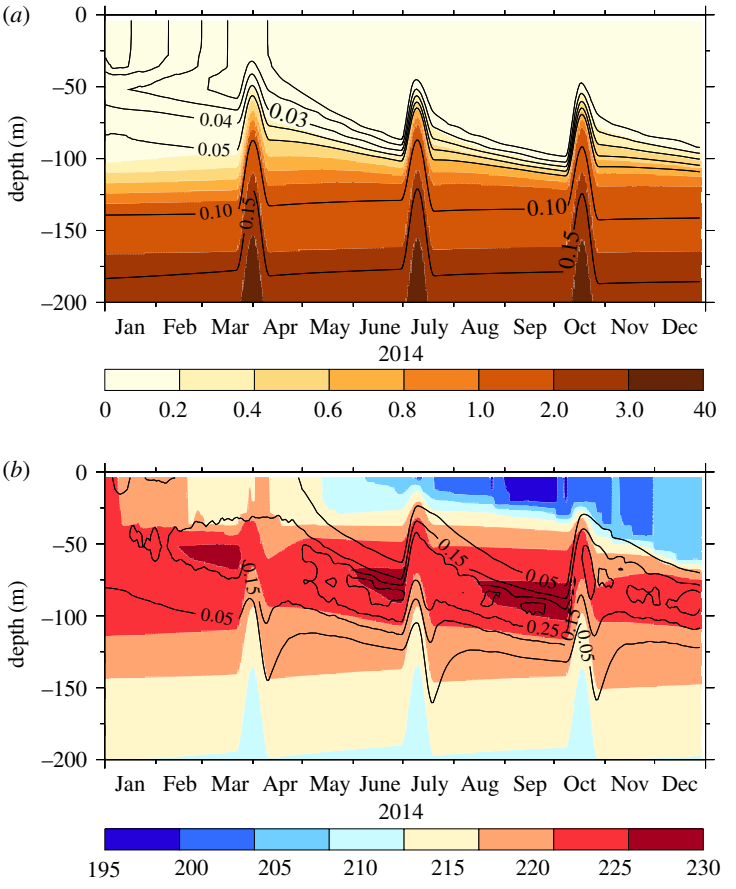

Figure 5. Reference simulation of nutrients, O_2 and chlorophyll *a*. (*a*) Distribution of nitrate (colours, mmol N m^{-3}) and phosphorus (contours, mmol P m^{-3}), (*b*) oxygen (colours, mmol O_2 m^{-3}) and chlorophyll *a* (contours, mg chl *a* m^{-3}). (Online version in colour.)

simulation. About 40% of the annual PP in the model solution is due to N_2 fixation, which occurs mainly during the first half of the year where there is a phosphorus excess due to mixing in late winter.

A relatively large fraction of organic material either sinks out of the euphotic zone or is transported into the deep as dissolved organic material and the combined oxygen consumption from either re-mineralized material or the oxygen debt of organic matter below 120 m accounts for 78% of PP (figure 6*b*). Most of the oxygen debt is due to the build-up of a small pool of dissolved organic carbon (DOC) of about 1–2 mmol C m^{-3} centred around the DCM (not shown) and, at the end of the year, the total pool of DOC corresponds to an oxygen consumption when re-mineralized of approximately 0.1 mol O_2 m^{-2}. The high export promotes the formation of a SOM in accordance with observations (figure 1). Other studies have also indicated a relatively large percentage of new production, i.e. high *f*-ratio in the North Atlantic subtropical gyre [2]. The model sensitivity to changes in the export ratio (i.e. the percentage of PP being exported, *e*-ratio) is analysed further below.

(iii) Deep chlorophyll maxima and eddy mixing

The dominant signals in the annual evolution of the phytoplankton biomass (chlorophyll *a*) occur in association with a deepening of the mixed layer during winter and passages of eddies during the more stratified period (figure 7). In early winter, nitrate is present in the upper surface

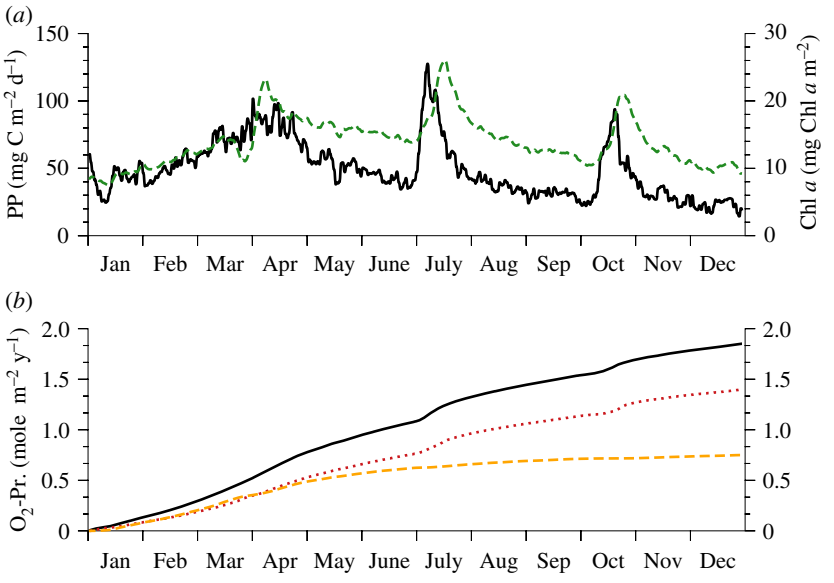

Figure 6. Time series of PP, chlorophyll *a* and O_2 production. Model solutions in the reference case of (*a*) primary production (PP, solid line) and vertically integrated chlorophyll *a* (dashed line). (*b*) Total accumulated oxygen production (solid line), O_2 production from N_2 fixation (dashed line) and oxygen equivalents from export and O_2 debt below 120 m (dotted line). (Online version in colour.)

layer. This leads to rapid growth of eukaryotic phytoplankton. The onset of a period of nitrate depletion at the end of January subsequently favours the development of diazotrophs and they then dominate the upper 50 m until the end of May when phosphate depletion results in more favourable conditions for phytoplankton growth to be located deeper in the water column. The eukaryotic phytoplankton form a DCM already at the end of March and the position of the DCM remains relatively deep during the rest of the year. Eddy passages result in an increase in eukaryotic phytoplankton as a result of the sudden surplus of nitrate higher in the water column and the corresponding decrease in both light and nutrient limitation on phytoplankton growth.

Diazotrophs dominate the upper part of the DCM where diffusive fluxes of phosphorus together with reduced light limitation provide a competitive advantage for these organisms. A model simulation without eddies shows that increased nutrient depletion during the season causes a gradual deepening of the DCM (figure 7*b*) and diazotrophs become less abundant in the autumn due to a lack of phosphorus. The maximum depth (approx. 125 m) of the DCM indicates that light limitation in the model is in general accordance with the observed maximum depth of the DCM (figure 3).

The role of nutrient limitation with respect to the position of the DCM in the water column was analysed further by comparing the reference case with a case where all organic material was either in particulate ($\delta_{DOM} = 0$) or dissolved form ($\delta_{DOM} = 1$). Increased nutrient depletion resulted in the DCM being located approximately 20 m deeper when all material was in particulate form whereas a more shallow and less well-defined DCM was established when all material went into DOM (figure 8). In this latter case, PP mainly took place in the upper 50 m of the water column and diazotrophs became more dominant owing to the competitive advantage from N_2 fixation and the relatively high phosphorus concentrations from recycled material. These results suggest that the presence of a deep DCM is related to a relatively large export of organic material.

(d) Sensitivity to ocean warming

The reference case was perturbed to consider potential effects from climate change on primary production and the oxygen budget (table 1). A likely consequence of a warmer ocean would be

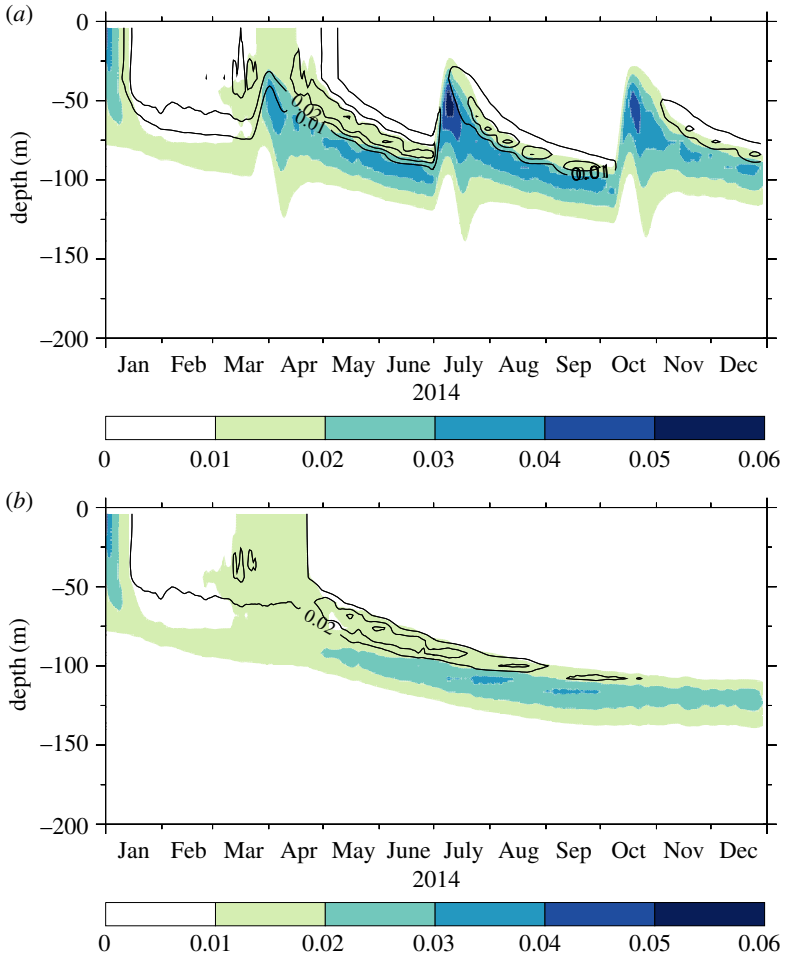

Figure 7. Eddies and DCM. Phytoplankton biomass of eukaryotes (P_1, colours, mmol N m^{-3}) and diazotrophs (P_2, contours, mmol N m^{-3}) in (*a*) the reference case with three passing eddies and (*b*) a case without eddies. (Online version in colour.)

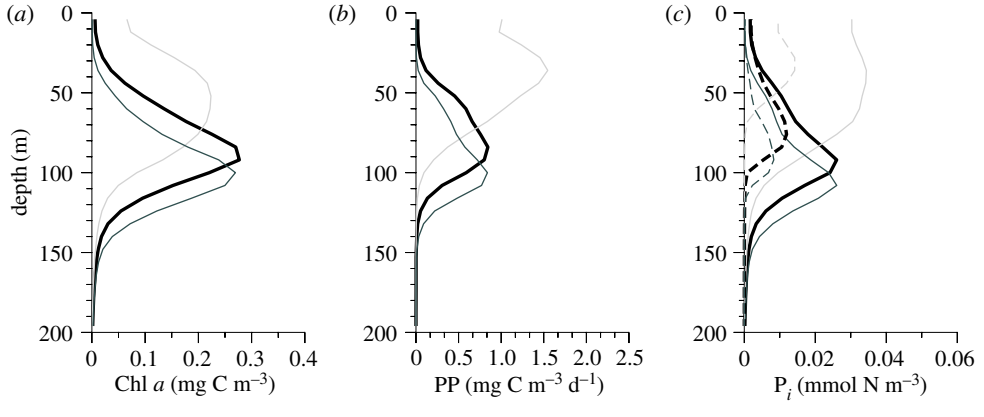

Figure 8. Sensitivity to DOM production. Averaged vertical profiles from May to November from the reference case (black), a case with no DOM production (light grey) and a case with only DOM production (i.e. no sinking material, dark grey). Profiles are shown for (*a*) chlorophyll *a*, (*b*) primary production and (*c*) distributions of eukaryotes (solid) and diazotrophs (dashed lines).

Table 1. Sensitivity to climate change.

exp.	O_2 production[a]	N_2 fixation[a]	*e*-ratio	re-mineralization 0–120 m[a]	O_2 debt 0–120 m[a]	⟨PP⟩[b]	⟨chl⟩[c]	description
1	1.85	0.75	0.75	0.41	0.10	48.8	14.0	reference case
2	1.88	0.69	0.74	0.45	0.09	49.7	14.0	increased re-mineralization rates (15%)
3	1.86	0.69	0.75	0.41	0.10	49.0	14.0	SST is increased by approximately 2°C
4	3.23	0.45	0.06	1.89	1.22	85.6	15.5	all organic material on dissolved form ($\delta_{DOM} = 1$)

[a]Annually accumulated value (mol O_2 m^{-2} yr^{-1}).
[b]Annually averaged PP (mg C m^{-2} d^{-1}).
[c]Annually averaged chlorophyll *a* (mg chlorophyll *a* m^{-2}).

increased re-mineralization of organic matter due to increased heterotrophic activity. Increasing the re-mineralization rates by 15% (i.e. corresponding to a temperature sensitivity $Q_{10} = 2$ and a temperature increase of 2°C) leads only to a minor increase (1%) in PP and correspondingly small changes in the oxygen budget. The limited influence of increased re-mineralization on PP is due to the high *f*-ratio where only a minor fraction of organic material remains in the surface layer.

In a case where the SST was increased by approximately 2°C (i.e. the atmospheric temperature in the surface forcing was increased by 2°C), PP was reduced by less than 1%. The model case we generate here actually induces a much larger change in stratification than would be expected in a future warmer climate where increased temperatures also would have penetrated deep into the upper ocean. Thus, the model suggests that PP in the Sargasso Sea will not be sensitive to climate change induced modification of stratification. Observational studies from the northern Atlantic subtropical gyre also show a weak correlation between PP and inter-annual variation in stratification [30].

The model solution does have a relatively high sensitivity to changes in the relative proportions of DOM and POM produced (table 1, exp. 4). If all organic matter is directed into the dissolved pool ($\delta_{DOM} = 1$) then the oxygen production increases by 75% and the *e*-ratio decreases to 6%, i.e. material is mainly transported deeper down due to advection and turbulent diffusion. Increased DOM relative to POM production caused by changes in planktonic food web structure has been suggested from mesocosm studies as a possible consequence of a warmer ocean [31]. Phytoplankton community structure has also been found to be sensitive to climate change in more complex ecosystem models [32], Therefore, sensitivity of the model processes to an altered fraction of produced DOM (δ_{DOM}), i.e. from zero (i.e. only POM) to 100% (i.e. only DOM), was explored.

Oxygen production increases significantly when all material is recycled in dissolved form because the nutrient concentrations increase in the surface layer (figure 9*a*). However, both re-mineralization and the O_2 debt, in the form of accumulated organic matter not yet re-mineralized, also increase. Therefore, net oxygen production in the upper 120 m decreases from 1.3 to 0.1 mol O_2 m^{-2} yr^{-1} when the fraction of DOM production increases from zero to 100% (i.e. the difference between the solid and black dashed lines in figure 9*a*). This also influences the oxygen flux deeper into the water column where the O_2 flux at 150 m is reduced from 0.30 to 0.18 mol m^{-2} yr^{-1} when δ_{DOM} changes from zero to one (figure 9*b*). Thus, an increased DOM production would tend to decrease the downward oxygen flux out of the euphotic zone by up to 40%. An increased DOM production would also tend to decrease the *e*-ratio (ranging from 93% to

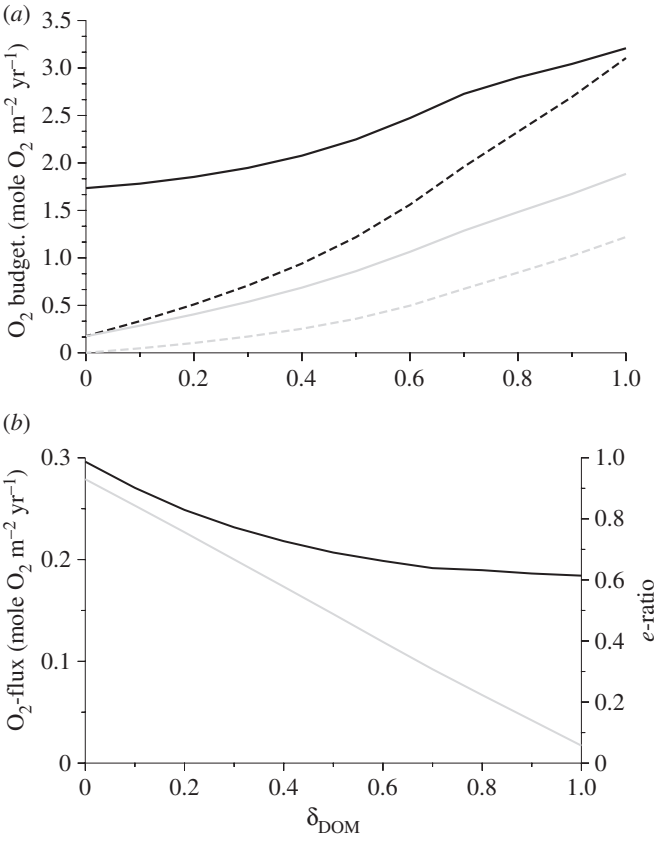

Figure 9. Sensitivity to DOM production. (*a*) Annually accumulated oxygen production (black, solid), re-mineralization (light grey), O_2 debt (dashed) in the upper 120 m and the sum of re-mineralization and O_2 debt above 120 m (black dashed line). (*b*) Downward oxygen flux at 150 m (black) and the corresponding *e*-ratio (light grey), i.e. production above 120 m versus export of organic material below 120 m.

6%, figure 9*b*) and this would tend to compensate the deep oxygen budget for the decreased oxygen flux across 150 m. The net effect in the upper ocean would, therefore, depend on the sinking and re-mineralization rates of particulate and organic material.

(e) Role of photosynthesis in water column oxygen flux

The roles of photosynthesis and mixing by eddies in oxygenation of the water column were analysed in three cases characterized by (I) no eddies, (II) anticyclonic eddies (lifting isopycnals) and (III) cyclonic eddies (deepening isopycnals) combined with different scenarios of biological production (table 2). In the simplest case, there were no eddies and no biological production. Here, the downward oxygen flux at 150 m was relatively low (0.04 mol O_2 m^{-2} yr^{-1}) and controlled only by the background turbulent diffusion. In this case, the oxygen flux was primarily regulated by the general oxygen difference between the surface and deep ocean.

Eddy mixing will tend to mix oxygen more efficiently. This can be demonstrated by removing biological production from the model and comparing the O_2 flux with and without eddies (table 2).

Increased oxygen in the SOM resulting from photosynthesis leads to a significant increase in the downward oxygen transport. In the case of mixing by cyclonic eddies, an overall increase of 56% in the downward oxygen flux at a depth of 150 m is found due to biologically produced oxygen. This effect is even more pronounced (i.e. an increase of 64%) when the reference case is

Table 2. Oxygen flux and eddy mixing.

description	biology	PP mg C m^{-2} d^{-1}	F_{O_2} (150 m) mol O_2 m^{-2} yr^{-1}
no eddies	none	0	−0.04
	$\delta_{DOM} = 0.2$	1.2	−0.04
	$\delta_{DOM} = 1.0$	1.9	−0.04
anticyclonic eddies	none	0	−0.14
	$\delta_{DOM} = 0.2$	1.5	−0.25
	$\delta_{DOM} = 1.0$	2.3	−0.18
cyclonic eddies	none	0	−0.23
	$\delta_{DOM} = 0.2$	1.2	−0.36
	$\delta_{DOM} = 1.0$	2.1	−0.25

modified to represent downwelling anticyclonic eddies because oxygen is now more efficiently transported deeper into the water column. In a case where organic matter is produced solely as DOM, the oxygen flux decreases because less oxygen is accumulated in the surface layer, i.e. the SOM is absent when there is no significant export.

These scenarios indicate that sub-surface photosynthetic oxygen production, in combination with relatively large eddy-induced vertical mixing, has the potential to significantly influence the downward oxygen transport in the area. The simulated oxygen flux at 150 m of about 0.3 mol O_2 m^{-2} yr^{-1} corresponds to about 1% of the total oxygen content in the upper 150 m. Although this is a minor flux compared with the ventilation of deep water masses at higher latitudes, it does suggest that photosynthesis at the base of the euphotic zone in the ocean's large subtropical gyres may contribute with significant amounts of oxygen to deeper ocean layers in these oligotrophic regions.

4. Conclusion

This study suggests that photosynthesis may be making a quantitatively important contribution to oxygenation of the water column in at least some of the permanently stratified oligotrophic regions of the global ocean. We are not aware of other studies in which the potential of photosynthesis in the water column O_2 flux has been considered. It is, however, generally assumed that the majority of water column photosynthesis takes place so close to the surface that upper ocean mixing processes in combination with ocean–atmosphere O_2 flux will prevent the retention of biologically produced O_2 in the ocean. The recognition deriving from empirical studies that significant new production may be taking place below the immediate surface layer, i.e. at the base of the euphotic zone, in some permanently stratified oligotrophic regions challenges this assumption. Indeed, the model study presented here not only suggests that sub-surface primary production makes a contribution to the ocean O_2 flux but also may account for substantial export production in these regions.

It is often argued [33–35] that ocean warming resulting from climate change will lead to a decrease in PP owing to more intense thermal stratification. In many coupled ocean–atmosphere Earth system models, this decrease in PP is assumed to lead to a reduction in export production and a resulting weakening of the ocean carbon sink [18]. The current study suggests, however, that the warming of the surface ocean layer will likely not lead to significant changes in the PP occurring in the Sargasso Sea. On the other hand, the study identifies eddy mixing as an important factor in the control of magnitude of photosynthesis here. One could envision that climate change might influence the intensity of eddies and/or the frequency of their passage but the direction of

these possible changes has not yet been identified. We suggest, nevertheless, that eddy behaviour may be a more likely candidate than changes in stratification for influencing PP, and therefore export production, in a warmer ocean in regions encompassed by the sub-tropical gyres.

Finally, this study suggests that the magnitudes of both the O_2 flux and export production occurring in the Sargasso Sea are highly sensitive to the relative proportion of particulate and organic material produced by photosynthesis. As this will in large part be a function of the planktonic food web structure and the species present in the community, this implies any changes that a warmer ocean may have on plankton biodiversity and the relative ratio of heterotrophic to autotrophic processes can potentially have important implications for the O_2 flux and export production here.

Data accessibility. CTD data are stored at the ICES Data Centre (http://www.ices.dk).

Authors' contributions. K.R. was responsible for the field studies and conducted the chemical/biological sampling. J.B. conducted the oceanographic field sampling. K.R. and J.B. developed the conceptual PP model. J.B. developed the mathematical model. Both authors contributed to writing the paper.

Competing interests. We declare we have no competing interests.

Funding. This investigation was supported by the Carlsberg Foundation (grant nos. 2012_01_0272 and 2013-01-0350) and the Danish National Science Foundation via its support of the Center for Macroecology, Evolution, and Climate (grant no. DNRF96). Ship time was funded by the Danish Center for Marine Research.

Acknowledgements. We thank captain and crew on R/V *Dana* for their assistance and Eik Ehlert Britch for technical support.

Appendix A

(a) Physical model

The model is based on the COHERENS model system [24] and is configured for a vertical 400 m deep water column with 50 equidistant layers. Surface forcing fields in the centre of the Sargasso Sea (65° W, 27° N) are obtained from NCEP reanalysis of meteorological fields [36] of air temperature, wind, relative humidity and cloudiness with a time resolution of 6 h in 2014. The model is integrated over 1 year starting from 1 January 2014 with a time step of 20 min and it is initialized from monthly WOA05 climatologies of temperature [37], nutrients, i.e. nitrate and phosphate [38], and oxygen [9]. Salinity is also included [39] by relaxing the salinity field towards the monthly climatology with a relaxation time scale of 10 days [40]. Thus, vertical variation in salinity is included in the calculation of stratification and, although it is relatively small, the indirect influence on vertical mixing is thereby considered (e.g. the influence from the high-saline Subtropical Underwater).

In a one-dimensional set-up, the COHERENS model solves the diffusion equation with specified sinks and sources. The one-dimensional set-up of the COHERENS model was extended with an advection operator so that the influence from passing eddies could be simulated explicitly. The vertical advection–diffusion equation (equation (2.1)) was thereby solved for all state variables with a specified vertical velocity due to eddies (w_{eddy}). Boundary conditions at the surface are specified from turbulent diffusive heat fluxes for temperature, a wind-dependent air–sea gas exchange for oxygen and zero fluxes for other state variables, and a no flux condition at the bottom for all state variables.

(b) Advection and eddy mixing

The vertical advection operator is based on the piecewise parabolic method (PPM) with monotonization [41]. The PPM is a fourth order advection scheme and resolves sharp vertical gradients with a small numerical diffusion. James [42] studied the PPM in a one-dimensional example of the time-dependent advection equation where it was assumed that there were no horizontal gradients of the state variable when vertical divergence required replacement with ambient fluid. Although the solution of equation (2.1) is more complex than the case studied

by [42] due to diffusive transports and the various source terms, a similar assumption of no horizontal gradients is assumed in the model set-up applied here. Thus, vertical divergence causes inflow of surrounding water with similar concentrations. This is a reasonable first-order description of transports due to diverging isopycnals in the upper ocean, because, in general, relatively small isopycnal gradients are observed of the state variables considered here. However, when contributions from other terms are included, as diffusion and internal sinks/sources (equation (2.1)), the replacement with ambient fluid implies a temporal change of concentrations, i.e. the concentration at a given level will change between the convergence and divergence of the isopycnal and, therefore, the solution will not be strictly mass conserving. Conservation of oxygen during an annual cycle in the model was analysed by accumulating air–sea exchange and total production and re-mineralization of O_2 and the relative difference (i.e. $\Delta O_2/\langle O_2\rangle$, where the total amount of oxygen $\langle O_2\rangle$ is approximately 85 mol in a 400 m water column) between a case with and without eddies of 5×10^{-4} was less than in a case without eddies between the initial O_2 and the final concentration of 8×10^{-4}. The difference between a case with eddies with and without biology was even less (2×10^{-4}). Therefore, we argue that mass conservation errors do not significantly affect the model solutions and oxygen fluxes discussed here.

The waiting time between passages of large mesoscale eddies in the Sargasso Sea is typically approximately 80 days or more and the propagation of the baroclinic Rossby waves is characterized by a westward velocity of approximately 4–5 km d^{-1} [43,44]. This is considered in the model by specifying a vertical eddy velocity; $w(z,t)=f(t)\ g(z)$. The time-dependence (f) is then zero when time is less than τ_{wait} (=80 days), i.e. the waiting time between two eddies, whereas the vertical eddy velocity is given by $f(t)=w_{max}\sin(\omega(t-\tau_{wait}))$ during an eddy passage, where w_{max} is the specified maximum vertical velocity. The period of the eddy is specified as $\omega=2\pi/\tau_{eddy}$, where the period of the eddy passage (τ_{eddy}) is assumed to be 20 days. If multiple eddy passages are considered, then the time is set to zero after the first eddy passage and the sequence is repeated. Initial upward displacements of isopycnals (i.e. cyclonic eddies) are considered in the reference case and the influence from downward displacements is considered in the sensitivity experiments. The vertical velocity structure of a mesoscale eddy is assumed to have a sinusoidal structure and to span the whole water column (i.e. $D=400$ m) with a maximum at mid-depth $g(z)=\sin(\pi\ z/D)$ and zero velocity at the surface and at the bottom of the water column. This parametrization is motivated by observations showing baroclinic eddies penetrating to great depths [45,46]. The maximum velocity (w_{max}) was specified to 10 m d^{-1} corresponding to an upward vertical displacement of 64 m at a depth of 200 m during the first 10 days (i.e. $\tau_{eddy}/2$), and in general accordance with isopycnal vertical displacements during passages of large mesoscale eddies [17] (figure 3*a*).

The potential influence from increased vertical mixing associated with eddy motion [16,46] is considered by adding an additional term to the vertical diffusion coefficient given by $k_v(\text{eddy})=k_v(e_{max})\ |w(z)|/w_{max}$ and the reference value of $k_v(e_{max})$ is assumed to be 5×10^{-4} m^2 s^{-1}. This value is comparable to observed values of vertical mixing associated with mesoscale eddies in the Sargasso Sea [4,16].

The explicit eddy parametrization makes it possible to study the direct effects from vertical advection associated with passages of mesoscale eddies on the biogeochemical cycling of nutrients. For example, lifting of isopycnals at the bottom of the euphotic zone causes increased light for phytoplankton during the eddy passage and increased eddy mixing will also alter the nutrient distribution. Thus, the simple eddy parametrization includes the most important aspects, in a general and simplified manner, of eddy passages for cycling of nutrients and oxygen.

Appendix B. Biogeochemical model

Sink and source terms in the transport equation (2.1) for the 10 biogeochemical state variables (figure 2) are specified as

Table 3. Photosynthetic parameters and chlorophyll : C ratios, $\eta_{\mathrm{Chla:C}}$, from the central Sargasso Sea from the Galathea 3 expedition in spring 2007 (average, standard error and no. of samples).

parameter	unit	surface (10 m)	DCM (less than 90 m)
$P^{\mathrm{B}}_{\mathrm{max}}$	$(\mu g\ C\ (\mu g\ Chl\ h)^{-1})$	$2.37 \pm 0.5\ (10)$	$0.96 \pm 0.2\ (8)$
α^{B}	$10^{-2}\cdot(\mu g\ C\cdot(\mu g\ Chl\ h\ \mu E\ m^{-2}\ s^{-1})^{-1})$	$1.37 \pm 0.2\ (10)$	$3.33 \pm 0.6\ (8)$
$\eta_{\mathrm{Chla:C}}$	$(\mu g\ Chl\ (\mu g\ C)^{-1})$	$0.02 \pm 0.03\ (15)$	$0.11 \pm 0.01\ (13)$

$$\frac{\partial A_1}{\partial t} = \eta_{\mathrm{N:C}}\mathrm{PP}_1 - mA_1 - G_1, \tag{B 1}$$

$$\frac{\partial A_2}{\partial t} = \eta_{\mathrm{N:C}}\mathrm{PP}_2 - mA_2 - G_2, \tag{B 2}$$

$$\frac{\partial N}{\partial t} = -\eta_{\mathrm{N:C}}\mathrm{PP}_1 + \frac{1}{\tau}(\mathrm{PON} + \mathrm{DON}) + \frac{1}{\tau_{\mathrm{C}}}\eta_{\mathrm{s}}^{-1}\mathrm{DOC}, \tag{B 3}$$

$$\frac{\partial P}{\partial t} = -\eta_{\mathrm{P:C}}(\mathrm{PP}_1 + \mathrm{PP}_2) + \frac{1}{\tau}(\mathrm{POP} + \mathrm{DOP}), \tag{B 4}$$

$$\frac{\partial \mathrm{PON}}{\partial t} = (1-\delta_{\mathrm{DOM}})m(A_1 + A_2) + (1-\gamma_{\mathrm{DOM}})(G_1 + G_2) - \frac{1}{\tau}PON - w_s\frac{\partial \mathrm{PON}}{\partial z}, \tag{B 5}$$

$$\frac{\partial \mathrm{DON}}{\partial t} = \lambda\delta_{\mathrm{DOM}}m(A_1 + A_2) + \lambda\gamma_{\mathrm{DOM}}(G_1 + G_2) - \frac{1}{\tau}\mathrm{DON}, \tag{B 6}$$

$$\frac{\partial \mathrm{POP}}{\partial t} = \eta_{\mathrm{P:N}}(1-\delta_{\mathrm{DOM}})m(A_1 + A_2) + \eta_{\mathrm{P:N}}(1-\gamma_{\mathrm{DOM}})(G_1 + G_2) - \frac{1}{\tau}POP - w_{\mathrm{s}}\frac{\partial \mathrm{POP}}{\partial z}, \tag{B 7}$$

$$\frac{\partial \mathrm{DOP}}{\partial t} = \eta_{\mathrm{P:N}}\delta_{\mathrm{DOM}}m(A_1 + A_2) + \eta_{\mathrm{P:N}}\gamma_{\mathrm{DOM}}(G_1 + G_2) - \frac{1}{\tau}\mathrm{DOP}, \tag{B 8}$$

$$\frac{\partial \mathrm{DOC}}{\partial t} = (1-\lambda)\eta_{\mathrm{s}}\delta_{\mathrm{DOM}}m(A_1 + A_2) + (1-\lambda)\eta_{\mathrm{s}}\gamma_{\mathrm{DOM}}(G_1 + G_2) - \frac{1}{\tau_{\mathrm{C}}}\mathrm{DOC} \tag{B 9}$$

and

$$\frac{\partial \mathrm{O}_2}{\partial t} = \eta_{\mathrm{O_2:C}}(\mathrm{PP}_1 + \mathrm{PP}_2) - \frac{1}{\tau}\eta_{\mathrm{O_2:N}}\mathrm{PON} - \frac{1}{\tau}\eta_l\mathrm{DON} - \frac{1}{\tau_{\mathrm{C}}}\mathrm{DOC}. \tag{B 10}$$

State variables are given in units of nitrogen, carbon and oxygen and their molar production and re-mineralization ratios are, for simplicity, assumed to be equal and their ratios (η) between P : N : C : O_2 are defined as: 1 : 16 : 106 : 138 [47].

Phytoplankton biomasses (A_1, A_2) are produced by primary production (PP_i, $i = 1,2$) and light-limited production (PP^{L}) is calculated according to [48]

$$\mathrm{PP}^L_i(z) = \mathrm{chl}_i(z)P^B_{\mathrm{max}}(z)\left(1 - \exp\left(\frac{-\mathrm{PAR}(z)\alpha^B(z)}{P^B_{\mathrm{max}}(z)}\right)\right), \tag{B 11}$$

where chl(z) and PAR(z) are the vertical (z) distribution of chlorophyll *a* and available photosynthetic light, respectively. PAR is calculated from incoming solar radiation at the surface and both self-shading from phytoplankton and attenuation in the red and blue part of the light spectrum is considered explicitly according to [49]. Our previous primary production measurements in the central Sargasso Sea in spring 2007 (Galathea 3 expedition, G3) provided photosynthetic parameters from the surface (10 m depth, $n = 33$) and from the DCM (average depth 120 m, $n = 16$) [50] and model values were linearly interpolated between the average values at these two depth levels (table 3).

Vertical variation of $\eta_{\mathrm{Chl}a:\mathrm{C}}$ has been found to be important for sustaining a DCM in numerical models of the Sargasso Sea [51]. Therefore, chlorophyll concentrations were obtained from phytoplankton biomasses and a vertically dependent chlorophyll *a* : carbon ratio ($\eta_{\mathrm{Chl}a:\mathrm{C}}$). Riemann *et al*. [11] found a large vertical variation in the central Sargasso Sea (also from G3) and average values of $\eta_{\mathrm{Chl}a:\mathrm{C}}$ from the stratified area south of 27° N ranged from 1/50 to 1/10 (in units of mg Chl $(\mathrm{mg\ C})^{-1}$) at the surface (10 m) and DCM (approx. 120 m), respectively (table 3).

Vertical variation of $\eta_{\mathrm{Chl}a:\mathrm{C}}$ in the model was then accounted for by linearly interpolating these average values between the two depth levels and assuming constant values above 10 m and below 120 m.

Primary production for the first phytoplankton group (A_1) is also assumed to be limited by both phosphate (P) and nitrate (N) through a Monod equation: $L^{\varphi} = \varphi/(k_{\varphi} + \varphi)$, $\varphi = \mathrm{N}$ or P. Thus, $\mathrm{PP}_1 = \mathrm{PP}_1^{\mathrm{L}} L^{\mathrm{P}} L^{\mathrm{N}}$, where the half saturation constants are defined as $k_{\mathrm{N}} = 0.01\ \mathrm{mmol\,m^{-3}}$ and $k_{\mathrm{P}} = \eta_{\mathrm{P:N}}\ k_{\mathrm{N}}$. The relatively low value of k_{N} resulted in a close coupling between nutrients and biomass and resulted in a DCM in accordance with observations. The second phytoplankton group was assumed to represent diazotrophs and their N_2-fixing ability made them only nutrient limited by phosphorus. However, nitrate assimilation was assumed to have a preference if nitrate concentrations were high and the PP_2 was, therefore, parametrized as: $\mathrm{PP}_2 = \mathrm{PP}_2^{\mathrm{L}} L^{\mathrm{P}}(1 - L^{\mathrm{N}})$, i.e. PP_2 was only dominant during nitrate-poor conditions.

Phytoplankton mortality rate (m) was defined by an e-folding time constant of 10 days and grazing was imposed on the two phytoplankton groups by a Holling-type III formulation: $G_i = g_0 A_i^2/(g_k + A_i^2)\ Z$, ($g_0 = 3.25\ \mathrm{d^{-1}}$, $g_k = 0.05\ \mathrm{mmol\,N\,m^{-3}}$) where the zooplankton biomass was assumed to be related with the phytoplankton biomass as: $Z = (A_1 + A_2)^{\gamma}$, $\gamma = 0.61$ [52].

Particulate (PON, POP) and dissolved (DON, DOP) fractions of nitrate and phosphate were produced from mortality and grazing, and the specified fraction from mortality (δ_{DOM}) and grazing (γ_{DOM}) divided the organic matter between the two pools ($\delta_{\mathrm{DOM}} = 0.2$ and $\delta_{\mathrm{DOM}} = \gamma_{\mathrm{DOM}}$). Labile organic matter is assumed to be re-mineralized back into its inorganic compounds with a time scale of $\tau = 10$ days [53,54] and particulate matter is assumed to sink through the water column with a constant sinking velocity ($w_s = 50\ \mathrm{m\,d^{-1}}$).

Observations and model studies from the Sargasso Sea [55] have shown a relatively high re-mineralization ratio in the upper 250 m with $\eta_{\mathrm{C:N}} \sim 19$, i.e. significantly higher than the Redfield ratio. Seasonal build-up of DOC [56] shows that 'less labile' organic carbon pools are re-mineralized on longer time scales. A semi-labile pool of DOC was, therefore, included with a longer re-mineralization time scale of 180 days. The dissolved organic nitrogen was divided between a labile ($\mathrm{DON_l}$) and semi-labile ($\mathrm{DON_s}$) pool by a fraction (λ); $\mathrm{DON} = \lambda\ \mathrm{DON} + (1 - \lambda)\ \mathrm{DON} = \mathrm{DON_l} + \mathrm{DON_s}$, and the semi-labile pool was assumed to have a higher C : N ratio (η_{s}) than the labile pool (η_{l}). Production of DON results in a corresponding oxygen production determined by $\eta_{\mathrm{O_2:N}}$, and this constrains the subsequent oxygen consumption during re-mineralization of DON, i.e. $\eta_{\mathrm{O_2:N}}\ \mathrm{DON} = \eta_{\mathrm{l}}\ \mathrm{DON_l} + \eta_{\mathrm{s}}\ \mathrm{DON_s}$, thus, the re-mineralization ratios of the two pools are related as: $\eta_{\mathrm{s}} = (\eta_{\mathrm{O_2:N}} - \eta_{\mathrm{l}}\lambda)\ /(1 - \lambda)$. We assume a small oxygen consumption of the labile pool given by $\eta_{\mathrm{l}} = 2$, corresponding to oxidation of ammonium to nitrate and, furthermore, we assume 60% of newly produced DON goes into the labile pool ($\lambda = 0.6$), and this results in a value of η_{s} of 18.6 in accordance with observed values [27]. However, these parameters are not directly constrained by observations and the build-up of a semi-labile pool is, therefore, discussed further in the sensitivity analysis. The semi-labile pool is described in terms of DOC and DOC production is then determined by η_{s} and a respiratory quotient of one. Oxygen (O_2) is produced by PP and consumed during re-mineralization of organic matter.

Sinking fluxes and the wind and solubility-dependent air–sea exchange of oxygen are updated separately whereas equations (B 1)–(B 10) are solved by a fourth-order Runge–Kutta algorithm with a biogeochemical time step of 300 s.

References

1. Polovina JJ, Howell EA, Abecassis M. 2008 Ocean's least productive waters are expanding. *Geophys. Res. Lett.* **35**, L03618. (doi:10.1029/2007GL031745)
2. Jenkins WJ, Goldman JC. 1985 Seasonal oxygen cycling and primary production in the Sargasso Sea. *J. Mar. Res.* **43**, 465–491. (doi:10.1357/002224085788438702)
3. Stanley RHR, Jenkins WJ, Doney SC, Lott DE. 2015 The ^{3}He flux gauge in the Sargasso Sea: a determination of physical nutrient fluxes to the euphotic zone at the Bermuda Atlantic Time-series Site. *Biogeosciences* **12**, 5199–5210. (doi:10.5194/bg-12-5199-2015)

4. Richardson K, Bendtsen J, Christensen JT, Adjou M, Lyngsgaard MM, Hilligsøe KM, Pedersen JB, Vang T, Nielsen MH. 2014 Localised mixing and heterogeneity in the plankton food web in a frontal region of the Sargasso Sea: implications for eel early life history? *Mar. Ecol. Prog. Ser.* **504**, 91–107. (doi:10.3354/meps10766)
5. Fawcett SE, Lomas MW, Ward BB, Sigman DM. 2014 The counter-intuitive effect of summer-to-fall mixed layer deepening on eukaryotic new production in the Sargasso Sea. *Glob. Biogeochem. Cycles* **28**, 86–102. (doi:10.1002/2013GB004579)
6. Dugdale RC, Goering JJ. 1967 Uptake of new and regenerated forms of nitrogen in primary productivity. *Limnol. Oceanogr.* **12**, 196–206. (doi:10.4319/lo.1967.12.2.0196)
7. Eppley RW, Peterson BJ. 1979 Particulate organic matter flux and planktonic new production in the deep ocean. *Nature* **282**, 677–680. (doi:10.1038/282677a0)
8. Riser SC, Johnson KS. 2008 Net production of oxygen in the subtropical ocean. *Nature* **451**, 323–326. (doi:10.1038/nature06441)
9. Garcia HE, Locarnini RA, Boyer TP, Antonov JI. 2006 In *World ocean atlas 2005*, vol. 3: *Dissolved oxygen, apparent oxygen utilization, and oxygen saturation* (ed. S Levitus), p. 342. NOAA Atlas NESDIS 63. Washington, DC: US Government Printing Office.
10. Emerson S. 2014 Annual net community production and the biological carbon flux in the ocean. *Glob. Biogeochem. Cycles* **28**, 14–29. (doi:10.1002/2013GB004680)
11. Riemann L, Nielsen TG, Kragh T, Richardson K, Parner H, Jakobsen HH, Munk P. 2011 Distribution and production of plankton communities in the subtropical convergence zone of the Sargasso Sea. I. Phytoplankton and bacterioplankton. *Mar. Ecol. Prog. Ser.* **426**, 57–70. (doi:10.3354/meps09001)
12. Lipschultz F, Bates NR, Carlson CA, Hansell, DA. 2002 New production in the Sargasso Sea: history and current status. *Glob. Biogeochem. Cycles* **16**, 1.1–1.17. (doi:10.1029/2000GB001319)
13. Painter SC, Patey MD, Forryan A, Torres-Valdes S. 2013 Evaluating the balance between vertical diffusive nitrate supply and nitrogen fixation with reference to nitrate uptake in the eastern subtropical North Atlantic Ocean. *J. Geophys. Res. Oceans* **118**, 5732–5749. (doi:10.1002/jgrc.20416)
14. McGillicuddy Jr DJ, Robinson AR, Siegel DA, Jannasch HW, Johnson R, Dickey TD, McNeil J, Michaels AF, Knap AH. 1998 Influence of mesoscale eddies on new production in the Sargasso Sea. *Nature* **394**, 263–266. (doi:10.1038/28367)
15. Oschlies A, Garcõn V. 1998 Eddy-induced enhancement of primary production in a model of the North Atlantic Ocean. *Nature* **394**, 266–269. (doi:10.1038/28373)
16. Ledwell JR, McGillecuddy Jr DJ, Anderson LA. 2008 Nutrient flux into an intense deep chlorophyll layer in a mode-water eddy. *Deep-Sea Res. II* **55**, 1139–1160. (doi:10.1016/j.dsr2.2008.02.005)
17. Johnson KS, Riser SC, Karl DM. 2010 Nitrate supply from deep to near-surface waters of the North Pacific subtropical gyre. *Nature* **465**, 1062–1065. (doi:10.1038/nature09170)
18. Ciais P *et al.* 2013 Carbon and other biogeochemical cycles. In *Climate change 2013: the physical science basis. Contribution of working group I to the fifth assessment report of the Intergovernmental Panel on Climate Change* (eds TF Stocker *et al.*). Cambridge, UK and New York, NY: Cambridge University Press.
19. Pedlosky J. 1990 The dynamics of the oceanic sub-tropical gyres. *Science* **248**, 316–322. (doi:10.1126/science.248.4953.316)
20. Grasshoff K, Ehrhardt M, Kremling K. 1983 *Methods of seawater analysis*, 2nd edn. Weinheim, Germany: Verlag Chemie.
21. Arar EJ, Collins CB. 1997 *Method 445.0. In vitro determination of chlorophyll a and pheophytin in marine and freshwater algae by fluorescence*. Washington, DC: US Environmental Protection Agency. www.epa.gov/microbes/m445_0.pdf.
22. Kolber ZS, Prasil O, Falkowski PG. 1998 Measurements of variable chlorophyll fluorescence using fast repetition rate techniques: defining methodology and experimental protocols. *Biochim. Biophys. Acta* **1367**, 88–106. (doi:10.1016/S0005-2728(98)00135-2)
23. From N, Richardson K, Mousing EA, Jensen PE. 2014 Removing the light history signal from normalized variable fluorescence (Fv/Fm) measurements on marine phytoplankton. *Limnol. Oceanogr. Methods* **12**, 776–783. (doi:10.4319/lom.2014.12.776)
24. Luyten P (ed.). 2014 *COHERENS—a coupled hydrodynamical-ecological model for regional and shelf seas: user documentation. Version 2.6*. Brussels, Belgium: Operational Directorate Natural Environment, Royal Belgian Institute of Natural Sciences.

25. Ledwell JR, Watson AJ, Law CS. 1993 Evidence for slow mixing across the pycnocline from an open-ocean tracer-release experiment. *Nature* **364**, 701–703. (doi:10.1038/364701a0)
26. Suggett DJ, Moore CM, Hickman AE, Geider RJ. 2009 Interpretation of fast repetition rate (FRR) fluorescence: signatures of phytoplankton community structure vs. physiological state. *Mar. Ecol. Prog. Ser.* **376**, 1–19. (doi:10.3354/meps07830)
27. Vassiliev IR, Prasil O, Wyman KD, Kolber Z, Hanson AK, Prentice JE, Falkowski PG. 1994 Inhibition of PS II photochemistry by PAR and UV radiation in natural phytoplankton communities. *Photosyn. Res.* **42**, 51–64. (doi:10.1007/BF00019058)
28. Beardall J, Young E, Roberts S. 2001 Approaches for determining phytoplankton nutrient limitation. *Aquat. Sci.* **63**, 43–69. (doi:10.1007/PL00001344)
29. de Boyer Montégut Madec CG, Fischer AS, Lazar A, Iudicone D. 2004 Mixed layer depth over the global ocean: an examination of profile data and a profile-based climatology. *J. Geophys. Res.* **109**, C12003. (doi:10.1029/2004JC002378)
30. Lozier SM, Dave AC, Palter JB, Gerber LM, Barber RT. 2011 On the relationship between stratification and primary productivity in the North Atlantic. *Geophys. Res. Lett.* **38**, L18609. (doi:10.1029/2011GL049414)
31. Wohlers J, Engel A, Zöllner E., Breithaupt P, Jürgens, K, Hoppe HG, Sommer U, Riebesell U. 2009 Changes in biogenic carbon flow in response to sea surface warming. *Proc. Natl Acad. Sci. USA* **106**, 7067–7072. (doi:10.1073/pnas.0812743106)
32. Boyd PW. 2015 Toward quantifying the response of the oceans' biological pump to climate change. *Front. Mar. Sci.* **2**, 77. (doi: 10.3389/fmars.2015.00077)
33. Hoegh-Guldberg O, Bruno JF. 2010 The impact of climate change on the world's marine ecosystems. *Science* **328**, 1523–1528. (doi:10.1126/science.1189930)
34. Steinacher M, Joos F, Frölicher TL, Bopp L, Cadule P, Doney SC, Gehlen M, Schneider B, Segschneider J. 2010 Projected 21st century decrease in marine productivity: a multi-model analysis. *Biogeosciences* **7**, 979–1005. (doi:10.5194/bg-7-979-2010)
35. Bopp L *et al.* 2013 Multiple stressors of ocean ecosystems in the 21st century: projections with CMIP5 models. *Biogeosciences* **10**, 6225–6245. (doi:10.5194/bg-10-6225-2013)
36. Kalney E *et al.* 1996 The NCEP/NCAR 40-year reanalysis project. *Bull. Am. Meteorol. Soc.* **77**, 437–471. (doi:10.1175/1520-0477(1996)077<0437:TNYRP>2.0.CO;2)
37. Locarnini RA, Mishonov AV, Antonov JI, Boyer TP, Garcia HE. 2006 In *World ocean atlas 2005*, vol. 1: *Temperature* (ed. S Levitus), p. 182. NOAA Atlas NESDIS 61. Washington, DC: US Government Printing Office.
38. Garcia HE, Locarnini RA, Boyer TP, Antonov JI. 2006 In *World ocean atlas 2005*, vol. 4: *Nutrients* (*phosphate, nitrate, silicate*) (ed. S Levitus), p. 396. NOAA Atlas NESDIS 64. Washington, DC: US Government Printing Office.
39. Antonov JI, Locarnini RA, Boyer TP, Mishonov AVGarcia HE 2006 In *World ocean atlas 2005*, vol. 2: *Salinity* (ed. S Levitus), p. 182. NOAA Atlas NESDIS 62. Washington, DC: US Government Printing Office.
40. Bendtsen J, Gustafsson KE, Petersen JK. 2006 Modelling vertical mixing in the surface boundary layer using artificial age tracers. *J. Mar. Syst.* **60**, 115–128. (doi:10.1016/j.jmarsys.2005.11.009)
41. Colella P, Woodward PR. 1984 The piecewise parabolic method (PPM) for gas-dynamical simulations. *J. Comput. Phys.* **54**, 174–201. (doi:10.1016/0021-9991(84)90143-8)
42. James ID. 2000 A high-performance explicit vertical advection scheme for ocean models: how PPM can beat the CFL condition. *Appl. Math. Model.* **24**, 1–9. (doi:10.1016/S0307-904X(99)00022-0)
43. Chelton DB, Schlax MG, Samelson RM. 2011 Global observations of nonlinear mesoscale eddies. *Prog. Oceanogr.* **91**, 167–216. (doi:10.1016/j.pocean.2011.01.002)
44. Clément L, Frajka-Williams E, Szuts ZB, Cunningham SA. 2014 Vertical structure of eddies and Rossby waves, and their effect on the Atlantic meridional overturning circulation at 26.5°N. *J. Geophys. Res. Oceans* **119**, 6479–6498. (doi:10.1002/ 2014JC010146)
45. Zhang Z, Zhang Y, Wang W, Huang RX. 2013 Universal structure of mesoscale eddies in the ocean. *Geophys. Res. Lett.* **40**, 3677–3681. (doi:10.1002/grl.50736)
46. Zhang Z, Tian J, Qiu B, Zhao W, Chang P, Wu D, Wan, X. 2016 Observed 3D structure, generation, and dissipation of oceanic mesoscale eddies in the South China Sea. *Sci. Rep.* **6**, 24349. (doi:10.1038/srep24349)

47. Redfield AC, Ketchum BH, Richards FA. 1963 The influence of organisms on the composition of sea water. In *The sea* (ed. MN Hill), pp. 26–77. New York, NY: Wiley-Interscience.
48. Webb WL, Newton M, Starr D. 1974 Carbon dioxide exchange of *Alnus rubra*. A mathematical model. *Oecologia* **17**, 281–291. (doi:10.1007/BF00345747)
49. Lévy M, Gavart M, Mémery L, CaniauxG, Paci A. 2005 A four-dimensional mesoscale map of the spring bloom in the northeast Atlantic (POMME experiment): results of a prognostic model. *J. Geophys. Res.* **110**, C07S21. (doi:10.1029/2004JC002588)
50. Richardson K, Bendtsen J, Kragh T, Mousing EA. 2016 Constraining the distribution of photosynthetic parameters in the Global Ocean. *Front. Mar. Sci.* **3**, 269. (doi:10.3389/fmars.2016.00269)
51. Ayata S-D, Lévy M, Aumont O, Sciandra A, Sainte-Marie J, Tagliabue A, Bernard O. 2012 Phytoplankton growth formulation in marine ecosystem models: should we take into account photo-acclimation and variable stoichiometry in oligotrophic areas? *J. Mar. Syst.* **125**, 29–40. (doi.org/10.1016/j.jmarsys.2012.12.010)
52. Adjou M, Bendtsen J, Richardson K. 2012 Modeling the influence from ocean transport, mixing and grazing on phytoplankton diversity. *Ecol. Model.* **225**, 19–27. (doi:10.1016/j.ecolmodel.2011.11.005)
53. Hopkinson HS, Vallino J, Nolin, A. 2002 Decomposition of dissolved organic matter from the continental margin. *Deep-Sea Res. II* **49**, 4461–4478. (doi:10.1016/S0967-0645(02)00125-X)
54. Bendtsen J, Hilligsøe K-M, Hansen JLS, Richardson K. 2015 Analysis of remineralisation, lability, temperature sensitivity and structural composition of organic matter from the upper ocean. *Prog. Oceanogr.* **130**, 125–145. (doi:10.1016/j.pocean.2014.10.00)
55. Ono S, Ennyu A, Najjar RG, Bates NR. 2001 Shallow re-mineralisation in the Sargasso Sea estimated from seasonal variations in oxygen, dissolved inorganic carbon and nitrate. *Deep-Sea Res. II* **48**, 1567–1582. (doi:10.1016/S0967-0645(00)00154-5)
56. Carlson CA, Ducklow HW, Michaels AF. 1994 Annual flux of dissolved organic carbon from the euphotic zone in the northwestern Sargasso Sea. *Nature* **371**, 405–408. (doi:10.1038/371405a0)